Sensors & Actuators: B. Chemical 417 (2024) 136136

Contents lists available at ScienceDirect

Sensors and Actuators: B. Chemical

journal homepage: www.elsevier.com/locate/snb

Multiplexed MicroRNA biomarker detection by bridging lifetime filtering imaging and dynamic chemical labeling

Maria Padial-Jaudenes [a,1,2], Mavys Tabraue-Chávez [b,1], Simone Detassis [c], Maria J. Ruedas-Rama [a], M. Carmen Gonzalez-Garcia [a,3], Mario Antonio Fara [b], F. Javier López-Delgado [b], Juan A. González-Vera [a], Juan J. Guardia-Monteagudo [b], Juan J. Diaz-Mochon [d,e,f], Emilio Garcia-Fernandez [a], Salvatore Pernagallo [b,*], Angel Orte [a,*]

[a] *Nanoscopy-UGR Laboratory. Departamento de Fisicoquímica. Unidad de Excelencia de Química Aplicada a Biomedicina y Medioambiente, Facultad de Farmacia, Universidad de Granada, Campus Cartuja, Granada 18071, Spain*
[b] *DESTINA Genomica S.L. Parque Tecnológico Ciencias de la Salud (PTS), Avenida de la Innovación 1, Edificio BIC, 18016, Granada, Spain*
[c] *OPTOI Srl, Via Vienna 8, Trento, 38121, Italy*
[d] *NanoChemBio Group. Departamento de Química Farmacéutica y Orgánica, Unidad de Excelencia de Química Aplicada a Biomedicina y Medioambiente, Facultad de Farmacia, Universidad de Granada. Campus Cartuja, Granada 18071, Spain*
[e] *GENYO Centre for Genomics and Oncological Research, Pfizer/University of Granada/Andalusian Regional Government. PTS Granada, Avenida de la Ilustración, 114, Granada 18016, Spain*
[f] *Instituto de Investigación Biosanitaria ibs.GRANADA, Granada, Spain*

ARTICLE INFO

Keywords:
MicroRNAs (miRs)
Biomarker detection
Dynamic chemical labeling
Luminescence imaging
Machine learning algorithms

ABSTRACT

MicroRNAs (miRs) have emerged as promising biomarkers for early disease diagnosis and personalized treatment monitoring. However, their clinical utility has been hampered by technical limitations. Dynamic chemical labeling (DCL) based on capturing abasic PNA probes and reactive nucleobases, known as SMART bases, is a PCR-free approach that has proven very useful for the direct interrogation of circulating miRs. In this work, we expand the palette of tools available for the detection of DCL miR by synthesizing a new SMART nucleobase called SMART-C-Eu. This nucleobase contains a stable lanthanide cryptate. Using this SMART-C-Eu base and time-gated (TG) luminescence imaging, we successfully detect and quantify miR-122–5p in human serum samples. miR-122–5p is a well-known biomarker for drug-induced liver injury. Through a bead-counting analysis approach, statistical robustness is improved and miR-122–5p concentrations are detected in the nanomolar range. Furthermore, we extend this approach to multiplexed detection of three different miRs (miR-371a-3p, miR-451a-5p, and miR-122–5p) using spectral and temporal filtering. Importantly, we designed a user-independent multiplexed analysis using machine learning algorithms for automatic bead classification. Although the sensitivity of this technique must be further improved to detect miRs at lower concentrations, the method represents a significant advancement in miR analysis by combining ML segmentation using lifetime and intensity images. In addition, the technique offers multiplexing capabilities and the potential for automation, paving the way for more accurate and robust clinical applications in the future.

1. Introduction

Over the past decade, exceptional attention has been placed on the search for new biomarkers in liquid biopsies to achieve early diagnosis and personalized monitoring of treatments. Among the biomarkers discovered in a variety of challenging diseases, microRNAs (miRs) have been particularly highlighted. miRs play pivotal regulatory roles in gene expression, encompassing gene suppression and posttranscriptional

* Corresponding authors.
E-mail addresses: salvatore@destinagenomics.com (S. Pernagallo), angelort@ugr.es (A. Orte).
[1] These authors contributed equally.
[2] Present address: Department of Nutrition and Sustainable Animal Production, Estación Experimental del Zaidín, Consejo Superior de Investigaciones Científicas, San Miguel 101, Armilla, E-18100 Granada, Spain
[3] Present address: Madrid Institute for Advanced Studies in Nanoscience (IMDEA Nanociencia), C/ Faraday 9, 28049 Madrid, Spain

https://doi.org/10.1016/j.snb.2024.136136
Received 1 March 2024; Received in revised form 17 May 2024; Accepted 11 June 2024
Available online 14 June 2024
0925-4005/© 2024 The Author(s). Published by Elsevier B.V. This is an open access article under the CC BY license (http://creativecommons.org/licenses/by/4.0/).

regulation [1,2]. The deregulation of circulating miR expression levels in body fluids has been associated with various conditions, such as different types of cancer [3–5], neurodegenerative disorders [6–8], and liver injuries [9]. For instance, in several studies, miR-122–5p (miR-122) has been identified as a potential biomarker for drug-induced liver injury (DILI) [10,11]. The distinctive expression patterns of serum or plasma miRs can serve as disease fingerprints, acting as diagnostic or prognostic biomarkers for various diseases [1,12]. miRs exhibit several characteristics of an ideal biomarker, as it shows specificity to the condition or pathology of interest, reliably indicates a disease before clinical symptoms appear (early detection), exhibits sensitivity to changes in pathology (monitoring disease progression or therapeutic response), and is easy to obtain from biological fluids [13].

Despite the significant potential of miRs as biomarkers, their use in clinical diagnostics has been constrained by the available analytical methods for their detection. Current methods present technical challenges for direct (extraction and amplification-free), accurate and robust detection and quantification of the usually low miR levels [4,14]. Regarding the latter, the standard techniques for miR analysis involve RNA extraction and are PCR-based [12], which show important limitations in terms of reproducibility, inability of quantifying isomiR and potential for translation to clinical diagnostics [14,15]. Other broadly used methods involve Northern blotting, microarrays or NGS [12,16,17]. Therefore, highly sensitive, extraction- and amplification-free detection techniques are urgently needed for the analysis of miRs in clinical samples, as well as precise data analysis methods [16,18,19]. In this context, luminescence-based platforms and hybridization-based methodologies stand out as significant approaches within the field.

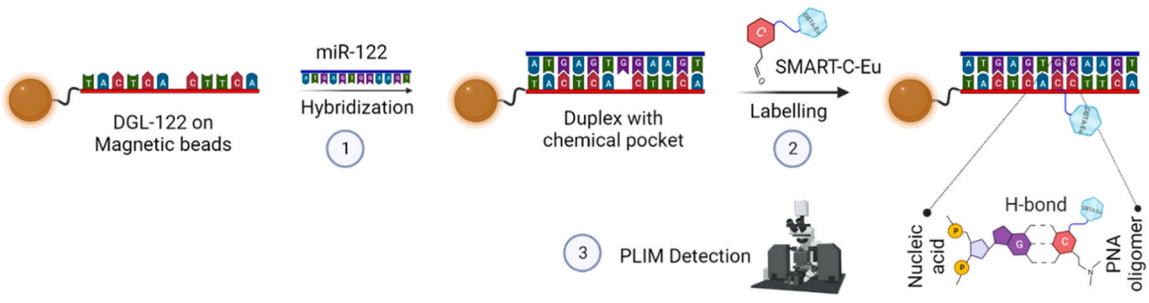
Dynamic chemical labeling (DCL) is a well-validated, PCR-free method for directly detecting miR direct with single-base resolution [5,20–28]. The method involves using abasic peptide nucleic acid (PNA) sequences, also known as DGL probes, that are complementary to the target nucleic acid and labeled with reactive nucleobases, SMART bases (SBs) [20,26,29]. The dynamic covalent chemical reaction occurs exclusively after fully complementary nucleic acid strands hybridize with DGL probes. The reaction occurs solely between the secondary amine of the DGL probe, which is located at the abasic position, and the reactive aldehyde group of the labeled SB (Scheme 1). This thermodynamically controlled reaction produces labeled DGL probe-miR duplexes that can be detected using various platforms [5,21–27,30]. A distinguishing characteristic of this technique is its ability to achieve a resolution of one base, which is not commonly found in the current published literature [31] and enables robust detection of single nucleotide variations (SNVs) [24–26].

Recently, we broadened and upgraded our detection platform portfolio through applying a time-gated (TG) luminescence imaging methodology by tagging luminophores with a long fluorescence lifetime [32]. This technique is particularly powerful when applied to complex samples, such as biological media and liquid biopsies; in these scenarios, undesired interference luminescence, such as scattered light, autofluorescence and impurities, can be reduced using the TG-filtered imaging approach [33]. This methodology has been applied to the study of miRs. For example, Hildebrandt *et al.* proposed a multiplexing technique using luminescence energy transfer (FRET) to analyze multiple miRs. The technique uses different FRET pairs and controls the energy donor-acceptor distance [34–37]. In their works, the luminescence lifetimes were in the nanosecond range due to the combination of quantum dots and organic fluorophores. A noteworthy group of luminophores for TG involves organometallic cryptates or inorganic nanoparticles with lanthanide ions that exhibit photoluminescence (PL) [33]. The emission of lanthanide ions typically has remarkably lengthy lifetimes, reaching even the millisecond time range for ions such as Eu(III) or Tb(III); this effect is primarily due to the emission originating from forbidden transitions [38], after an antenna-driven energy transfer [39]. By using biotin-europium-tagged streptavidin [40] or lanthanide-doped nanoparticles [41,42], researchers have recently developed miR sensors based on the PL emission of lanthanide ions.

Given the rising interest in lanthanide-based TG imaging [43], in this study, we merged DCL and TG imaging filtering approaches to identify multiple circulating miRs using a lanthanide-cryptate SB. This new method significantly broadens the spectrum of time windows available for the TG imaging analysis of various miRs. As a result, multiplexing capabilities are promoted and miR fingerprint patterns are generated for more reliable and precise clinical applications.

2. Material and methods

To expand the methods available for miR detection and quantification to PL lifetime imaging (PLIM) using the DCL methodology, a new SMART nucleobase was synthesized (SMART-C-Eu, Figure S1 in the Supplementary Materials, SM[72]), including the lanthanide cryptate DTBTA-Eu –{2,2',2'',2'''-{4'-{[(4,6-dichloro1,3,5-triazin-2-yl)amino] biphenyl-4-yl}-2,2':6',2''-terpyridine6,6''-diyl}bis(methylenenitrilo)} tetrakis(acetato)} europium (III)– as a very stable lanthanide luminophore [44]. The SMART-C-Eu base (Figure S1) was synthesized, purified to over 95 % purity, and characterized by DESTINA Genomica SL (Spain) following the synthetic route described elsewhere [20]. The PNA-based DGL probes were also synthesized, purified, and characterized as described elsewhere [24,26], achieving over 90 % purity. RP-HPLC is used to purify and characterise both SBs and DGL probes, and HRMS (ES+) and MALDI-TOF were used as mass spectroscopy techniques to characterize SBs and DGL probes, respectively. Table S1 in the SM shows the sequences of the DGL probes. The DGL probes were coupled with superparamagnetic beads with a diameter of 2.8 μm, presenting carboxylic acid groups (Dynabeads M-270, Thermo Fisher Scientific). The coupling protocol was previously optimized by our group [5,22], and is based on the coupling reaction of the beads carboxylic acids with the DGL probes using activation with 1-ethyl-3-(3-dimethylaminopropyl)carbodiimide (EDC). A solution containing the DGL capture probe and an amino-terminated diluent DNA sequence was added to the activated beads. The mixture was incubated, washed, and the probe coupling was measured using UV, resulting in ~600,000 probes/bead, and ensuring lot-to-lot reproducibility. Finally, the beads were stored in a solution of 10 % PEG10K and 0.1 % Tween-20 in PBS



Scheme 1. Capturing and labeling target miR-122 with the SMART-C-Eu nucleobase for detection using PLIM.

buffer. SBs and beads containing DGL probes were provided by DESTINA Genomica SL (Spain).

DCL was performed as previously described [5,20–28,30,32]. Briefly, 5×10^5 Dynabeads M-270 carboxylic acid (Thermo Fisher) coupled with DGL-miR122 probes were incubated for 1 h with 25 μL of proprietary lysis buffer and either 10 μL of commercial human serum (Sigma Merck) with synthetic DNA oligo miR-122 spike-ins (to prepare the calibration curve) or 10 μL of serum from DILI patients. Subsequently, washes with 0.1 % PBS-T were performed via a Biotek washer, and DCL was performed by incubating SMART-C-Eu, DCL buffer (2× SSC, 0.1 % SDS, pH 6) and 1 mM sodium cyanoborohydride (Sigma Merck) in a total volume of 50 μL for 1 h. After DCL, washings were performed as described above before microscopy measurements. SMART-C-FAM and SMART-C-Cy5 have been reported elsewhere [45].

For multiplex experiments, 5×10^5 Dynabeads M-270 carboxylic acid coupled with either DGL-miR122 probes, DGL-miR-371a probes, or DGL-miR-451a were incubated for 1 h with 5 μL of synthetic DNA oligo (miR-122–5p; miR-371a-3p; miR-451–5p) and 45 μL of DCL buffer (three distinct assays). After DCL, washings were performed as described above before microscopy measurements. For multiplexing detection of the DCL assays, a single solution encompassing 1:1:1 of reacted DGL-miR-122, DGL-miR451a and mDGL-miR371a was created before measuring with PLIM.

2.1. Instrumentation

Steady-state fluorescence emission spectra were obtained on a Jasco FP-8300 Spectrofluorometer (Jasco, Tokyo, Japan). Time-resolved luminescence spectra were collected using a Varian Cary Eclipse fluorescence spectrophotometer using the following conditions: excitation wavelength 320 nm; total decay time 15.0 ms; delay time 0.1 ms; gate time 0.2 ms; and number of flashes 50.

PLIM was performed on an Abberior Expert Line confocal PLIM microscope (Abberior, Germany) equipped with a fast quad galvanometer scanner. The excitation source was a pulsed, 375 nm laser, working at a frequency of 20 MHz. The PL images were collected in two different temporal windows. For millisecond PL emission of the DTBTA-Eu luminophore, a train of pulses of the 375 nm laser for 200 μs was employed for the excitation, followed by a 5 ms detection time window. The emission of DTBTA-Eu was detected on an avalanche photodiode (APD) detector after a 605/50-nm bandpass filter. For nanosecond fluorescence emission of the luminophores Cy5 and FAM, we simultaneously employed 488 nm and 635 nm pulsed excitation lasers, working at a 20 MHz repetition rate. The Cy5 PL emission was collected on an avalanche photodiode detector with a 685/70-nm bandpass filter, whereas the FAM PL emission was collected on a Hybrid PMT with a 510/20-nm bandpass filter. Single photon time-tagging and the reconstruction of nanosecond PL decay traces were performed on a HydraHarp 400 photon counting module (PicoQuant, Germany).

2.2. Image analysis

Analysis of PLIM images was performed using SymphoTime 64 (Picoquant, Germany) and home-coded scripts in Fiji (distribution of ImageJ) [46]. SymphoTime 64 was employed to reconstruct PLIM images in the nanosecond time window of Cy5 and FAM from their respective detection channels. Once reconstructed, we performed comprehensive PLIM imaging analysis by pixelwise fitting of the PL decay traces to a single exponential function. PLIM images from DTBTA-Eu in the millisecond time frame were not fitted because only the PL intensity was of interest; hence, no lifetime information was recovered in the DTBTA-Eu channel. The specific image analysis methodology for bead counting and multiplexing applications is described below.

2.3. Patient samples

Serum samples were provided by DESTINA Genomica SL through the University of Edinburgh. Samples were collected from patients and healthy volunteers. Full informed consent was obtained from the participants, and ethical approval was given by the Southeast Scotland Research Ethics Committee and the East of Scotland Research Ethics Committee via the Southeast Scotland Human Bioresource as a part of the MAPP (markers and paracetamol poisoning) study [10]. Samples were collected and prepared as described elsewhere [47].

3. Results and discussion

3.1. Incorporation of the SMART-C-Eu nucleobase for labelling miR-122

First, we characterized the emission properties of the newly synthesized SMART-C-Eu nucleobase. The PL emission spectra of purified SMART-C-Eu exhibited the characteristic emission peaks of Eu(III) (Figure S1) and showed a PL lifetime, τ, of 1.09±0.07 ms, in agreement with the reported value of 1.06 ms [48]. These results confirm that the linkage reaction with the nucleobase did not alter the emissive properties of DTBTA-Eu.

Once SMART-C-Eu was successfully obtained, we tested the performance of this reagent for the well-established DCL methodology to label miRs. For this, we employed miR-122 as the target biomarker. We designed a capture and labeling method using magnetic beads carrying the PNA-based DGL-122 capturing probe and the subsequent DCL reaction with the SMART-C-Eu nucleobase (Scheme 1). After the reaction, the beads carrying the labeled target miR-122 were imaged using PLIM microscopy. As mentioned above, the main advantage of combining PLIM microscopy and the millisecond luminescence emission of Eu(III) is that background- and interference-free images can be generated using time-gated (TG) filtering [33].

The success in the reaction for capturing and detecting miR-122 using the SMART-C-Eu nucleobase was first tested using control samples of miR-122 in an aqueous buffer. Fig. 1 shows representative time-gated PL (TG-PL) intensity images of individual beads after the DCL reaction with increasing concentrations of miR-122. The images show that nM concentrations can be easily detected and the TG-PL emission intensity and the concentration of miR-122 are correlated. Linear fitting resulted in a limit of detection of 1.4 nM [estimated as the concentration equivalent to 3×(s.d.) of the blank].

3.2. Optimization of the PLIM analysis settings and beadwise analysis

Once we established the concentration-dependent detection of miR-122 using the DCL reaction and the new SMART-C-Eu nucleobase, we enhanced the statistical robustness of our method using a beadwise image analysis approach. The ratio of DGL probes captured within the beads and the actual concentration of target miR may result in a statistical distribution of hybridized duplexes over the imaged beads. This factor is especially important when the target miR is at very low concentrations. For example, a beadwise analysis with single molecule sensitivity was needed for target miR at down to fM levels, as shown by our group previously [5,24,26]. Low miR copy numbers may result in many 'blank' beads carrying only a few target molecules if any. Therefore, we improved the method by studying the emitted TG-PL intensity distribution in individual beads. For this, we extended our field of view (FoV) to 50×50 μm^2 and fostered an increase in the number of beads in the FoV by using an external magnet (Fig. 2**A**). We then performed confocal imaging under continuous irradiation (to identify beads due to their autofluorescence emission) and PLIM imaging of the FoV. We implemented a home-scripted routine in Fiji that performed the following steps (see SM for the complete script): i) the Otsu threshold criterion [49] was applied as an automatic intensity threshold to the bead autofluorescence image; ii) individual beads were identified and

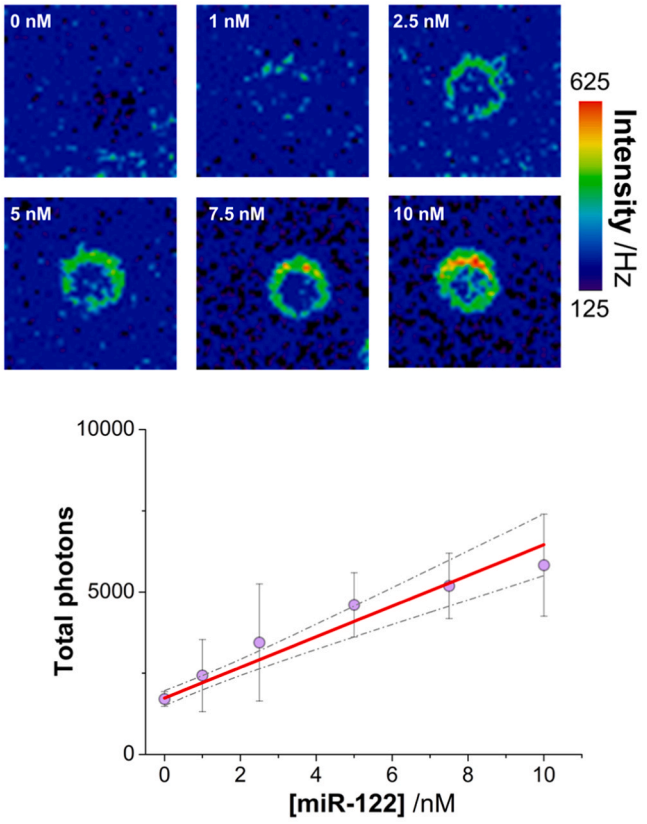


Fig. 1. TG-PL intensity images of individual beads after the DCL reaction using the SMART-C-Eu nucleobase with different concentrations of miR-122 in aqueous buffer. A threshold of 250 Hz was employed for pixel segmentation and photon counting. All images are 10×10 μm^2. The total number of detected photons per bead showed a linear dependency on the concentration of miR-122. Error bars represent s.d. from at least 3 images of individual beads.

segmented by the particle analyzer tool [46], after the watershed tool was applied to separate beads in close proximity; and iii) the average TG-PL intensity and bead area (defined as the μm^2 of the selected region of interest, ROI, for individual particles, i.e. beads) in each segmented particle was measured. Once the code is executed, the results from ROIs smaller than 30 pixel^2 were discarded, because they may correspond to incomplete beads or abnormally bright pixels. With these results, we built bead intensity distributions and correlated bead intensity with the corresponding bead area. Fig. 2**B** compares bead intensity values of a control sample and the DCL analysis of a 1.5 nM miR-122 test sample in aqueous buffer. Fig. 2**C** shows the beadwise intensity distribution of three different samples. The reproducibility of our results is supported by the fact that very similar populations are obtained in independent samples (represented as different symbols in Fig. 2C). Using the negative samples, we estimated a threshold value for considering positive beads. The average DTBTA-Eu intensity per bead in the negative beads was 124 ±16 Hz. Hence, we established a threshold value of 172 Hz (= $<I>_{negative}$ + 3·s.d.) to determine if a bead carries sufficient miR-122. Fig. 2C shows that, overall, three different samples of 1.5 nM miR-122 resulted in an average of 25 % positive beads, whereas the blank samples yielded 0.6 % positive beads. Positive beads are represented in red in Fig. 2C. This classification criterion offers a bead-counting approach to reliably identify the likelihood of a bead carrying detectable amounts of target miR-122, even at low concentrations. Importantly, the image analysis process can be automated using optimized criteria for thresholding and particle detection, yielding user-independent results.

3.3. Calibration in human serum

We then implemented this methodology in human serum test samples spiked with varying amounts of miR-122. Due to the numerous other components found in complex biological fluids, transitioning to human serum samples is difficult; however, DCL technology is perfectly suited for this task.

Fig. 2F shows a response calibration batch from 0 to 1.6 nM spiked-in miR-122 in human serum samples. We also compared the beadwise intensity distributions of all the samples (Fig. 2**E**), clearly showing the concentration-dependent signal in terms of average luminescence intensity per bead. As performed with the samples in the aqueous buffer, we employed negative beads to establish a threshold value of $<I>_{negative}$ + 3·s.d., which was 256 Hz, slightly larger than that in aqueous solution, possibly due to nonspecific adsorption of SMART-C-Eu nucleobases and the presence of low levels (1–5 pM range) of naturally occurring miR-122 [24]. We quantified the percentage of positive beads for each sample (including three repetitions for each), shown as red symbols in Fig. 2E. Importantly, the percentage of positive beads showed a correlation with the overall miR-122 concentration in serum samples (Fig. 2F), allowing us to quantify miR-122 levels in the nM range.

3.4. Detection of miR-122 in patient samples

Once the detection in serum was tested, we detected abnormal levels of miR-122 in the serum of patients with drug-induced liver injury (DILI). We performed the beadwise analysis described above for two aliquots of serum from a DILI patient and compared the results with two samples of healthy individuals. As shown in Fig. 3, the number of positive beads in a DILI patient serum was 9.4 % and 11.9 % for the two repetitions, respectively, whereas it was 1 % or 0.1 % for the healthy patients. Overall, the whole population of beads of DILI samples, with average intensity values of 225.8±1.4 Hz (s.e.m.) and 220.2 ± 0.8 Hz (s.e.m.), were shifted to higher intensity values than samples from healthy individuals, exhibiting intensity values of 194.8 ± 1.6 Hz (s.e.m.) and 188.4 ± 0.8 Hz (s.e.m.). Statistical comparison of the populations resulted in robust statistically significant differences between the DILI and healthy samples (p values between 10^{-54} and 10^{-102}). This result clearly demonstrates the potential of our method to detect overexpressed levels of miR-122 in patients. By interpolating the percentage of positive beads in the calibration (Fig. 2**F**), we obtained concentrations of 0.9 ± 0.2 nM and 1.0 ± 0.2 nM, respectively. This high concentration is consistent with the quantification performed by other techniques for these samples, including gold-standard qPCR, which yielded miR-122 concentrations on the order of 700 pM [21,26].

3.5. Multiplexed detection of different miRs using time-gated analysis

As mentioned in the previous sections, DTBTA-Eu cryptate exhibits a luminescence lifetime of 1.09 ms. Interestingly, this provides new possibilities for multiplexing by using different analysis time windows in TG imaging. The ms-lived luminescence emission of DTBTA-Eu occurs in a completely different photon stream than conventional ns-lived fluorophores. A time-resolved image analysis with such different detection windows would enable error-free multiplex detection while avoiding any photon cross-talk. Herein, we tested this concept by optimizing a multiplexing detection of three different miRs using spectral and lifetime filtering tools. We combined the methodology described above for miR-122 analysis with two additional capturing beads containing a DGL probe (Table S1 in the SM) for miR-371a-3p (miR-371), a well-validated biomarker for germ cell tumors [50–52], and miR-451a-5p (miR-451), an erythroid cell-specific miR [53] and potential biomarker in cancer and therapeutic activity [54]. For the DCL reaction, we employed specific SB nucleobases carrying fluorescein (FAM) for miR-371 and Cy5 for miR-451. These two well-known organic luminophores emit fluorescence on the nanosecond time scale with lifetime values of τ_{FAM} =

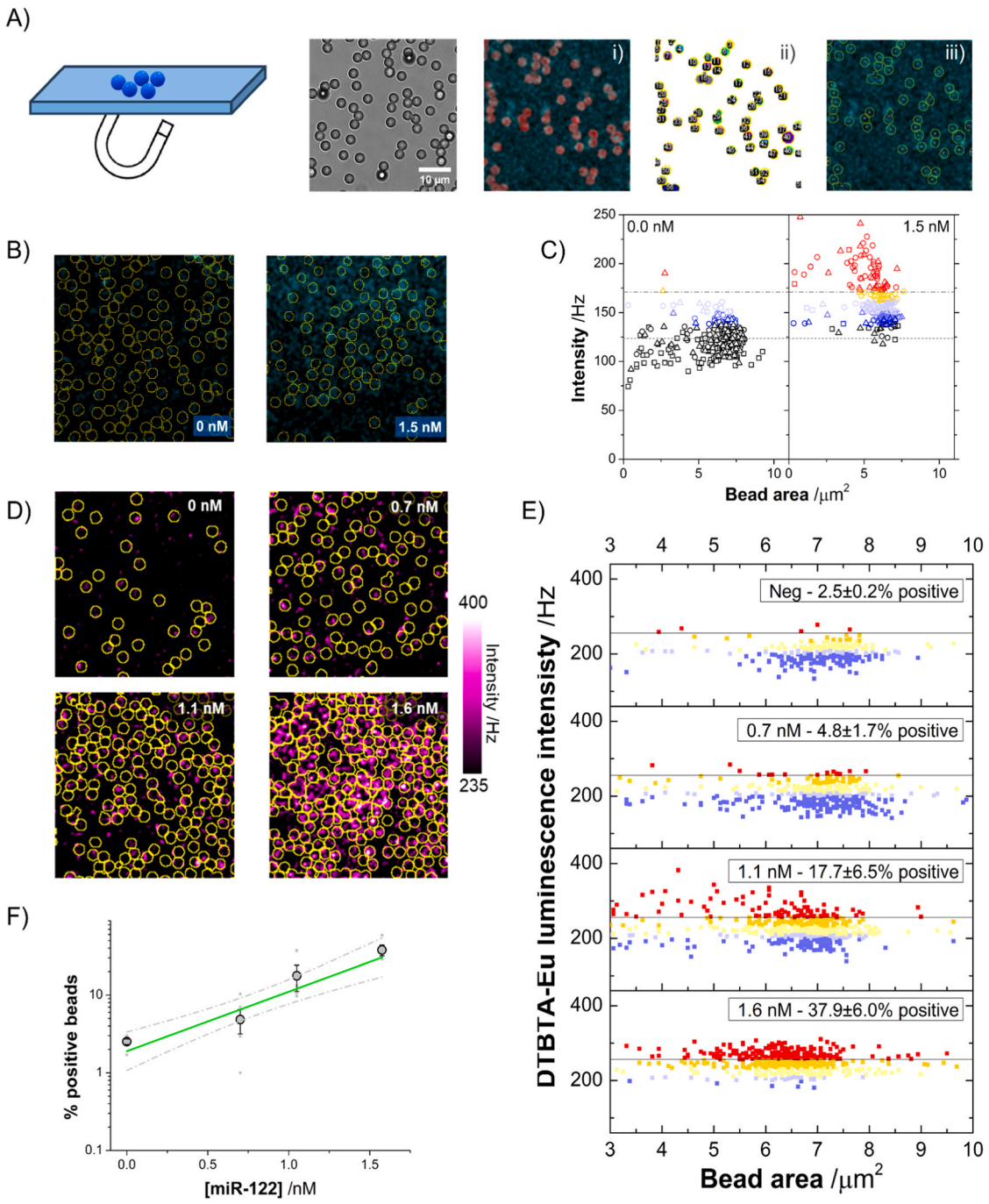


Fig. 2. A) Using a magnet, the beads are concentrated in the FoV for confocal imaging, as shown in the brightfield image. Then, beadwise analysis and readout were performed as follows: i) Overlap of direct fluorescence bead image, $\lambda_{ex} = 375$ nm, $\lambda_{em} = 685/70$ nm (red) and TG-PL imaging of DTBTA-Eu, $\lambda_{ex} = 375$ nm, $\lambda_{em} = 595/50$ nm (cyan). ii) Bead identification and segmentation using the bead fluorescence image. iii) Once the ROIs are selected, the average TG-PL intensity per bead is read out. B) TG-PL images of 50×50 µm^2 FoVs of beads after the DCL reaction with 0 or 1.5 nM of miR-122 in aqueous buffer. Yellow ROIs indicate bead identification using the procedure described. C) TG-PL intensity *versus* bead area from three different samples (identified as different symbols) of 0 and 1.5 nM of miR-122 in aqueous buffer. The dotted gray line indicates the $\langle I \rangle_{negative}$ value, whereas the dash-dotted line indicates the $\langle I \rangle_{negative} + 3\times$(s.d.) threshold value. Symbols above the threshold are shown in red. D) TG-PL images of 50×50 µm^2 FoVs of beads after the DCL reaction with different concentrations of miR-122 spiked in human serum samples. Yellow ROIs indicate bead segmentation. E) TG-PL intensity *versus* bead area from different concentrations of miR-122 spiked in human serum samples (at least three different repetitions). The horizontal line indicates the $\langle I \rangle_{negative} + 3\times$(s.d.) threshold value in serum samples. Symbols above the threshold are shown in red. F) Correlation of the percentage of positive beads *versus* the concentration of miR-122 in human serum samples. Error bars indicate s.d. Small gray dots indicate the values obtained from the individual samples. The green line is a linear fit (on the semilogarithmic scale), and the gray dash-dotted lines indicate the confidence limits at the 95 % confidence level.

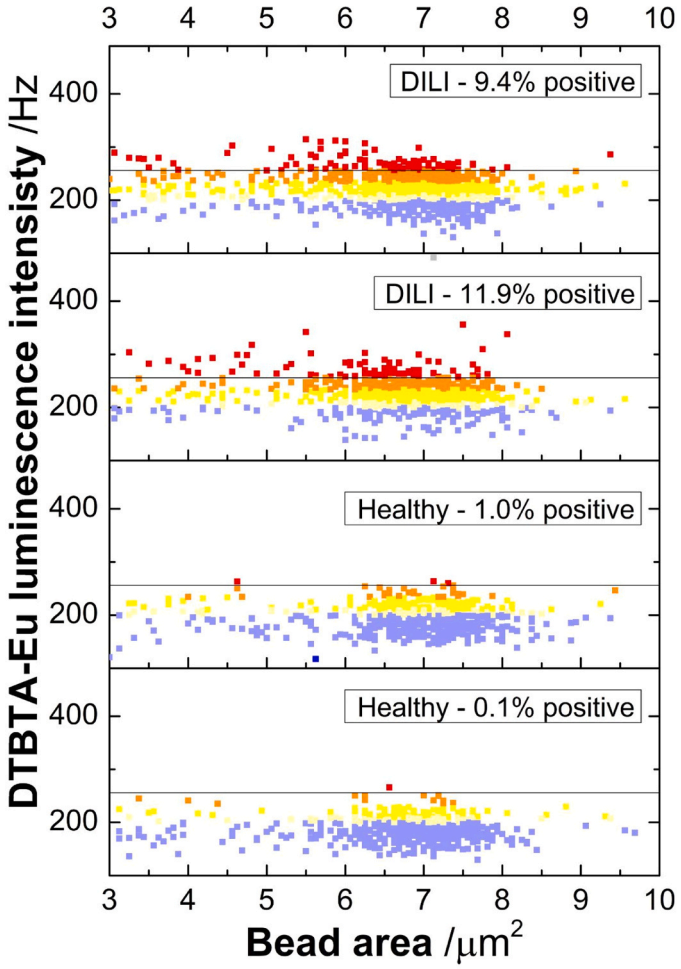


Fig. 3. Bead counting analysis, correlating TG-PL intensity of DTBTA-Eu *versus* the bead area from serum samples of DILI patients or healthy individuals from 10 different 50×50 μm^2 FoVs containing beads. The color heatmap indicates the luminescence intensity, with orange dots indicating values > 234 Hz ($<I>_{negative}$ + 2×(s.d.)) and red dots indicating values > 256 Hz ($<I>_{negative}$ + 3×(s.d.)), the latter set as the threshold for counting positive beads. The percentage of positive beads for each sample is indicated in the inset.

4.16 ns and τ_{Cy5} = 1.07 ns [55,56], respectively. Hence, we used different excitation schemes and spectral and temporal filtering (Fig. 4) to obtain the following orthogonal layers of information: i and ii) intensity and ns-PLIM images from FAM; iii and iv) intensity and ns-PLIM images from Cy5; and v and vi) intensity and ms-PLIM images from DTBTA-Eu.

For these experiments, samples containing spiked miRs (10 nM) were incubated with the corresponding capture beads carrying the DGL probes, and the DCL labeling reaction with the different corresponding SMART bases was carried out. Then, the beads were centrifuged and washed to remove excess reactant SMART, and the three were mixed at a 1:1:1 ratio. For calibration and optimization, experiments with one type of bead were performed. Multiplexed imaging acquisition (Fig. 4) consisted of ns-PLIM on a green detector for FAM (miR-371) and a far-red detector for Cy5 (miR-451) and a subsequent ms-PLIM acquisition, with a 5 ms detection time window, on a red detector for DTBTA-Eu (miR-122). Pixelwise fitting to a single exponential function was performed on the FAM and Cy5 images resulting on the actual ns-PLIM images, containing lifetime information. Positive beads for miR-371 were defined as those with lifetime values above 1.4 ns in the FAM image, and positive beads for miR-451 were defined as those with lifetime values above 0.8 ns in the Cy5 image (Fig. 5). For the DTBTA

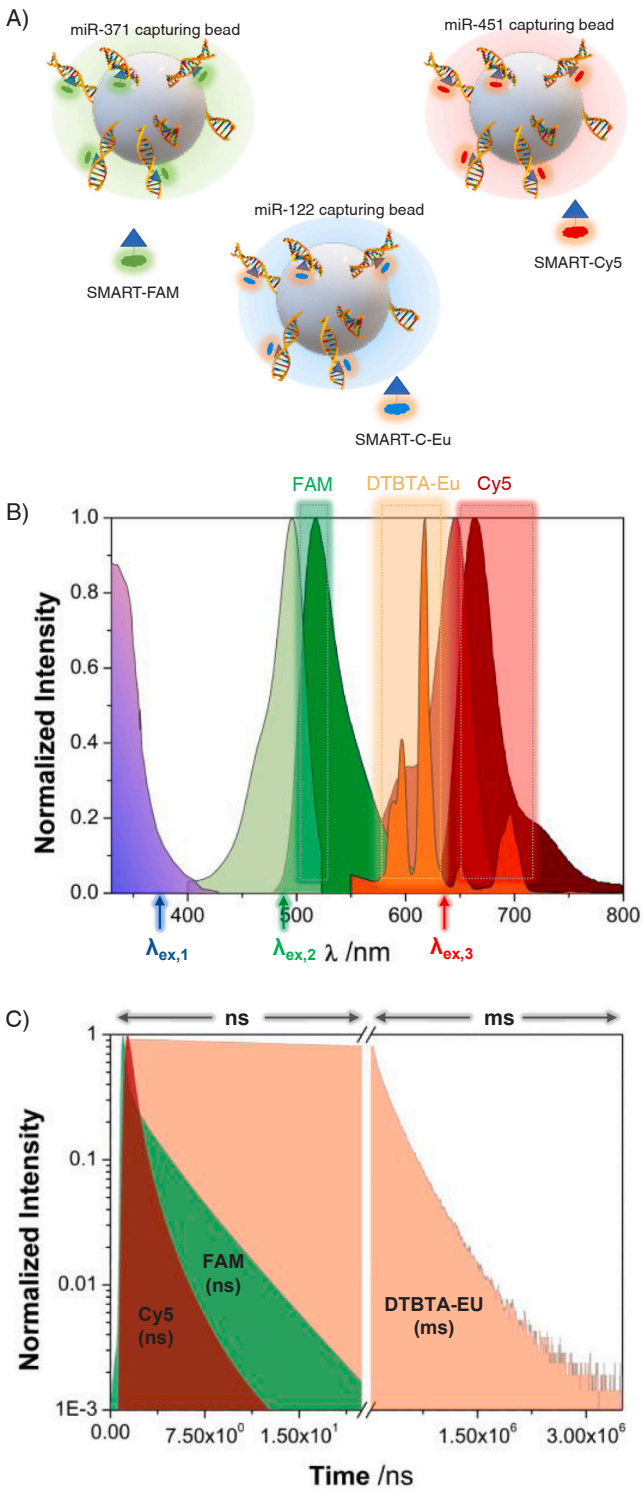


Fig. 4. A) Scheme of the multiplexed analysis of miR-371, miR-451 and miR-122 using DGL capturing probes in magnetic beads and three different SBs. The different spectra and analysis time windows are shown in panels B) and C).

channel, we obtained ms-PLIM images but reconstructed the TG-PL image by applying a filtering TG window. As explained earlier, this process achieves images that are totally free from other sources of luminescence emission apart from DTBTA-Eu. The composite image of the three types of beads was reconstructed, an automatic, unsupervised thresholding and particle analysis was performed, and the average intensity per bead in each channel was read out. The samples positive for the three types of miRs (see Figure S2 for further examples) showed well-

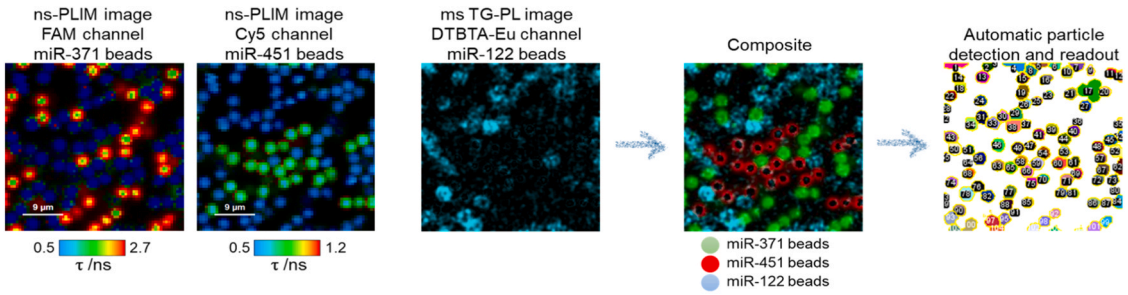


Fig. 5. Process for lifetime and TG bead classification. The ns-PLIM images in the FAM channel and the Cy5 channel are shown in a pseudocolor scale. Beads were classified as positive for miR-371 when $\tau > 1.4$ ns in the FAM channel and positive for miR-451 when $\tau > 0.8$ ns in the Cy5 channel. These two images were then composited with that obtained from the millisecond-range TG-PL image (from DTBTA-Eu). The ms TG-PL image contained only TG-filtered intensity information. The automatic particle segmentation procedure was applied for bead counting, classification and intensity readout in each channel.

separated populations (Figure S3). Appropriate negative controls (Figure S4) and controls of samples containing just one type of miR (Figure S5) showed the robustness of the automatic analysis method, as no misclassification or cross identification of beads was observed.

The composite images, containing intensity values in the three channels, were then analyzed using different machine-learning (ML) algorithms of classification and clustering. First, we used supervised machine learning to train particle classifiers with measurements of samples containing only one of the miRs as training dataset (Fig. 6 and Figure S5). Different algorithms were tested (k nearest neighbor, K-nn; support vector machines, SVM; decision trees; and random forest) by using partitions of the training dataset and cross-validating the classification results using 10 different random iterations. All algorithms tested except one resulted in similar performance (see Table 1), and the K-nn algorithm generated the best figures. Then, the trained algorithms were applied to all images of the 1:1:1 mixture, containing beads that carried each of the labeled miRs. The correlation plots in Fig. 6 show the color-coded classification of beads. The overall quantification of all the images using the trained K-nn algorithm yielded 30 % positive beads for miR-371, 23 % positive beads for miR-451 and 47 % positive beads for miR-122. The larger number of beads containing miR-122 may occur

Table 1
Performance parameters of the different supervised ML classification algorithms. The whole dataset consisted of 871 beads containing miR-451 // Cy5, 563 beads containing miR-122 // DTBTA-Eu, and 478 beads containing miR-371 // FAM. The training dataset was randomly selected in each iteration, maintaining the abundance distribution of the different classes. Ten different iterations were performed for cross-validation.

ML algorithm	Accuracy	Cohen's κ
K-nn	99.61 %	0.994
SVM	53.55 %	0.370
Decision Tree	99.22 %	0.988
Random Forest	99.50 %	0.992

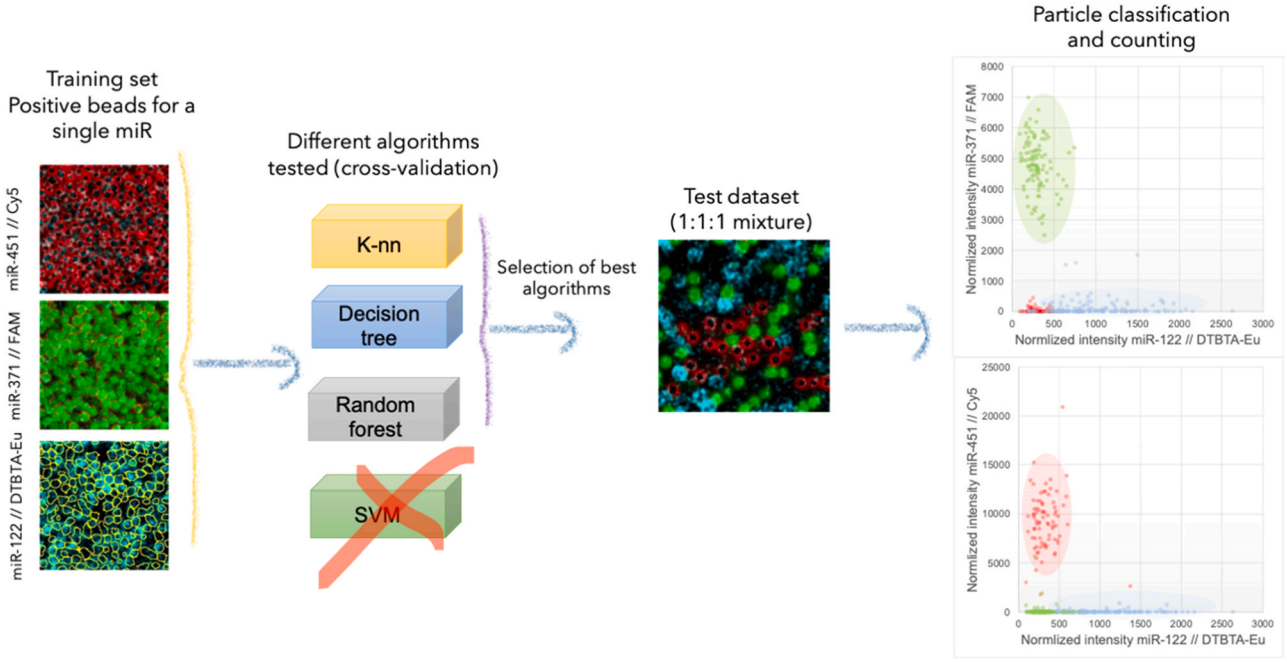


Fig. 6. Approach of supervised ML classification of beads. The training set was composed of 15 different images containing positive beads of each type, miR-451// Cy5, miR-371//FAM, or miR-122//DTBTA-Eu, for a total of 1802 beads. The different ML algorithms were trained by randomly splitting the beads in the training/test dataset 90 %/10 %, cross-validating the performance with 10 different repetitions. The performance figures for each algorithm in Table S2 are the average values from the 10 iterations. Once the algorithms were trained, they were applied to the images of the 1:1:1 mixture (5 images, 403 detected beads) for bead classification and counting. The correlation plots show the intensity in the FAM (top) or the Cy5 (bottom) channel *vs.* the intensity in the DTBTA-Eu channel for each bead. Each point corresponds to one bead, color-coded according to the classification obtained by the K-nn algorithm as miR-451//Cy5 (in red), miR-371//FAM (in green), or miR-122//DTBTA-Eu (in cyan).

because there were more beads in the stock solution before mixing. The robustness of the ML analysis algorithms is demonstrated by the excellent accuracy figures when applied to test datasets, with a very low fraction of misclassified events (Table 1).

We also tested an unsupervised ML clustering algorithm by using only the images of the 1:1:1 mixture. We used the k-means clustering algorithm, the overall intensities on each channel needed to be normalized for the algorithm to work successfully. As shown in Fig. 7, the k-means clustering algorithm satisfactorily defined three different clusters of beads. The centroids of these clusters, defined by the average normalized intensity in the Cy5 (I_{Cy5}), FAM (I_{FAM}) or DTBTA-Eu ($I_{DTBTA-Eu}$) channels, respectively, were as follows: i) $I_{Cy5} = 0.002$, $I_{FAM} = 0.014$, $I_{DTBTA-Eu} = 0.337$; ii) $I_{Cy5} = 0.450$, $I_{FAM} = 0.006$, $I_{DTBTA-Eu} = 0.089$; and iii) $I_{Cy5} = 0.004$, $I_{FAM} = 0.686$, $I_{DTBTA-Eu} = 0.080$. Clusters i, ii and iii corresponded to miR-122//DTBTA-Eu beads, miR-451//Cy5 beads, and miR-371//FAM beads, respectively. All the beads from the analyzed images were counted and according to the cluster classification, yielded 30 % of positive beads for miR-371, 22 % of positive beads for miR-451 and 48 % of positive beads for miR-122; these results corresponded perfectly with the results obtained using the supervised learning algorithm.

4. Discussion

By introducing the novel SMART-DTBTA-Eu nucleobase, we have expanded the palette of luminescence techniques available for DCL-based detection of miRs to ms-TG filtering of the reporting signal and imaging. In addition, the development of this reagent has facilitated an elegant method involving multiplexing for the simultaneous detection of three different miRs using PLIM microscopy and different time windows for analysis, ranging from nanoseconds to milliseconds. This method for multiplexing using bead barcoding can pave the way to larger panels of miR screenings with clinical applications [16,57].

Notably, in the proposed procedure, the samples are analyzed directly without a preamplification step. Our detection limit is comparable to other recent amplification-free methodologies employed for miR quantification [58]. While miR-122 levels in DILI patients are detectable using the presented methodology, other miRs used as significant biomarkers usually exhibit much lower expression levels, even reaching fM concentrations [14,47]. Ultrasensitive electrochemical detection of miRs at levels as low as pM or even fM has been achieved [19,59–61], but careful laboratory control is necessary for maintaining the optimal functionality of these devices.

Although our methodology has progressed, its sensitivity can be improved for the detection of biomarkers other than miR-122 in patients with DILI. Therefore, with other miRs, we suggest using universal and random amplification as an initial step in our approach, allowing for multiple distinctions with a precise resolution of a single nucleotide. Rolling circle amplification (RCA) shows promise as a potential preamplification technique [61,62]. Following RCA, techniques that employ highly sensitive PL emission and TG have been proposed for miR analysis, reaching detection limits as low as subfM levels [36]. Other recent amplification methods for miR detection involve the use of DNAzymes, such as catalytic hairpin assembly [63], hybridization chain reaction [64], or combining exonuclease I and tyramine signal amplification [65], leading to sub-fM limits of detection. Moreover, amplification cycles have even allowed detection of miR expression inside living cells and organoids [66,67]. However, all these methods are based on measuring fluorescence intensity changes.

While few amplification-free methods can analyze miR using PL, choosing the right luminophores [68] or employing single-molecule techniques [24,69] can lower the detection limit to pM levels. Other potential issues with our methodology include the requirement for specialized equipment and training. Nonetheless, recent advances in ultrafast cameras, which can be integrated into pre-existing commercial microscopes to enable PLIM [70], will lead to automated, high-throughput PLIM screening [71]. In any case, the strength of our method currently lies not in its sensitivity but in its specificity and multiplexing capabilities via lifetime-filtering imaging in different detection time windows.

5. Conclusions

In this study, we broadened the range of techniques available for the dynamic labeling of miRs using SMART bases in the DCL reaction. A novel SMART nucleobase containing a DTBTA-Eu luminophore was successfully synthesized for millisecond TG and PLIM analysis. This newly developed reagent effectively detects and quantifies miR-122 in serum samples as a DILI biomarker through an automated, straightforward, analyst-independent analysis. The primary goal of this study was to demonstrate a proof of concept for multiplexed PLIM with varying analysis time windows, from nanosecond to millisecond detection windows, using the DCL method. We also evaluated the proficiency of supervised and unsupervised ML algorithms for automatically classifying beads as a proof of concept for reliable and automated analysis. The combination of lifetime and intensity layers in ML-driven segmentation is a powerful, novel concept of our approach.

Our team plans to create a universal method of quickly increasing RNA amounts to be integrated into the analytical process described in this study. We strongly believe that identifying multiple miR biomarkers using DCL and TG imaging filtering shows potential and is suitable for creating a new, advanced miR analysis system, particularly when combined with a universal and random preamplification process. This method provides an opportunity for straightforward and resilient future multiplex assessments through which multiple miR biomarkers with predictive value can be examined in illnesses such as liver damage and cancer.

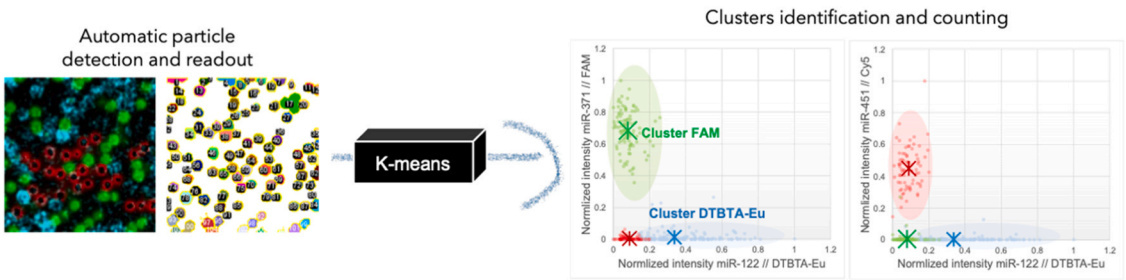


Fig. 7. Approach involving the unsupervised ML clustering of beads. The images of the 1:1:1 mixture (5 images, 403 beads) were fed to the K-means algorithm (with 3 potential clusters), having previously normalized the intensity values in each channel between 0 and 1. The correlation plots show the intensity in the FAM (left) or the Cy5 (right) channel *vs.* the intensity in the DTBTA-Eu channel for each bead. Each point corresponds to one bead, color-coded according to the cluster assigned by the K-nn algorithm as miR-451//Cy5 (in red), miR-371//FAM (in green), or miR-122//DTBTA-Eu (in cyan). The centroid values for each of the identified clusters are shown as crosses.

CRediT authorship contribution statement

Mavys Tabraue-Chávez: Resources, Methodology, Investigation. **Angel Orte:** Writing – review & editing, Writing – original draft, Visualization, Supervision, Software, Project administration, Methodology, Funding acquisition, Formal analysis, Data curation, Conceptualization. **Maria Padial-Jaudenes:** Investigation, Formal analysis. **Salvatore Pernagallo:** Writing – review & editing, Writing – original draft, Supervision, Resources, Project administration, Methodology, Funding acquisition, Conceptualization. **Maria J. Ruedas-Rama:** Writing – review & editing, Supervision, Methodology, Investigation, Formal analysis. **Simone Detassis:** Writing – review & editing, Methodology, Investigation. **Juan J. Guardia-Monteagudo:** Resources, Methodology, Investigation. **Juan A. González-Vera:** Writing – review & editing, Methodology, Investigation, Funding acquisition, Conceptualization. **Emilio Garcia-Fernandez:** Writing – review & editing, Supervision, Investigation, Formal analysis, Conceptualization. **Juan J. Diaz-Mochon:** Writing – review & editing, Supervision, Methodology, Funding acquisition, Conceptualization. **M. Carmen Gonzalez-Garcia:** Investigation, Formal analysis. **F. Javier López-Delgado:** Resources, Methodology, Investigation. **Mario Antonio Fara:** Writing – review & editing, Resources, Methodology, Investigation.

Declaration of Competing Interest

The authors declare the following financial interests/personal relationships which may be considered as potential competing interests: Salvatore Pernagallo reports a relationship with Destina Genomica SL that includes: employment and equity or stocks. Juan J. Diaz-Mochon reports a relationship with Destina Genomica SL that includes: board membership and equity or stocks. Simone Detassis reports a relationship with OPTOI Srl that includes: employment. If there are other authors, they declare that they have no known competing financial interests or personal relationships that could have appeared to influence the work reported in this paper.

Data Availability

Datasets from the manuscript can be found at Digibug repositoire at DOI: 10.30827/Digibug.84916

Acknowledgements

This work has been funded by the European Union through the Horizon 2020 diaRNAgnosis project, under grant agreement No. 101007934; and Agencia Estatal de Investigación (Spain) through grant PID2020-114256RB-I00 AEI/10.13039/501100011033 and grant CTQ2017-85658-R AEI/10.13039/501100011033/FEDER "Una manera de hacer Europa". Funding for open access charge: Universidad de Granada / CBUA. Additionally, the author thanks Prof. James Dear for his invaluable scientific guidance on the miR-122 biomarker.

Appendix A. Supporting information

Supplementary data associated with this article can be found in the online version at doi:10.1016/j.snb.2024.136136.

References

[1] C.E. Condrat, D.C. Thompson, M.G. Barbu, O.L. Bugnar, A. Boboc, D. Cretoiu, N. Suciu, S.M. Cretoiu, S.C. Voinea, miRNAs as biomarkers in disease: latest findings regarding their role in diagnosis and prognosis, Cells 9 (2) (2020) 276, https://doi.org/10.3390/cells9020276.

[2] J. Wang, J. Chen, S. Sen, MicroRNA as biomarkers and diagnostics, J. Cell. Physiol. 231 (1) (2016) 25–30, https://doi.org/10.1002/jcp.25056.

[3] S. Detassis, V. del Vescovo, M. Grasso, S. Masella, C. Cantaloni, L. Cima, A. Cavazza, P. Graziano, G. Rossi, M. Barbareschi, L. Ricci, M.A. Denti, miR375-3p Distinguishes Low-Grade neuroendocrine from non-neuroendocrine lung tumors in FFPE Samples, Front. Mol. Biosci. 7 (2020), https://doi.org/10.3389/fmolb.2020.00086.

[4] S. Detassis, M. Grasso, V. Del Vescovo, M.A. Denti, microRNAs make the call in cancer personalized medicine, Front. Cell Dev. Biol. 5 (86) (2017), https://doi.org/10.3389/fcell.2017.00086.

[5] S. Detassis, M. Grasso, M. Tabraue-Chávez, A. Marín-Romero, B. López-Longarela, H. Ilyine, C. Ress, S. Ceriani, M. Erspan, A. Maglione, J.J. Díaz-Mochón, S. Pernagallo, M.A. Denti, New platform for the direct profiling of micrornas in biofluids, Anal. Chem. 91 (9) (2019) 5874–5880, https://doi.org/10.1021/acs.analchem.9b00213.

[6] P. Piscopo, M. Grasso, V. Manzini, A. Zeni, M. Castelluzzo, F. Fontana, G. Talarico, A.E. Castellano, R. Rivabene, A. Crestini, G. Bruno, L. Ricci, M.A. Denti, Identification of miRNAs regulating MAPT expression and their analysis in plasma of patients with dementia, Front. Mol. Neurosci. 16 (2023), https://doi.org/10.3389/fnmol.2023.1127163.

[7] P. Piscopo, M. Grasso, M. Puopolo, E. D'Acunto, G. Talarico, A. Crestini, M. Gasparini, R. Campopiano, S. Gambardella, A.E. Castellano, G. Bruno, M. A. Denti, A. Confaloni, Circulating miR-127-3p as a potential biomarker for differential diagnosis in frontotemporal dementia, J. Alzheimer'S. Dis. 65 (2018) 455–464, https://doi.org/10.3233/JAD-180364.

[8] M. Grasso, P. Piscopo, A. Confaloni, M.A. Denti, Circulating miRNAs as biomarkers for neurodegenerative disorders, Molecules 19 (5) (2014) 6891–6910, https://doi.org/10.3390/molecules19056891.

[9] P.J. Starkey Lewis, J. Dear, V. Platt, K.J. Simpson, D.G.N. Craig, D.J. Antoine, N. S. French, N. Dhaun, D.J. Webb, E.M. Costello, J.P. Neoptolemos, J. Moggs, C. E. Goldring, B.K. Park, Circulating microRNAs as potential markers of human drug-induced liver injury, Hepatol 54 (5) (2011) 1767–1776, https://doi.org/10.1002/hep.24538.

[10] J.W. Dear, J.I. Clarke, B. Francis, L. Allen, J. Wraight, J. Shen, P.I. Dargan, D. Wood, J. Cooper, S.H.L. Thomas, A.L. Jorgensen, M. Pirmohamed, B.K. Park, D. J. Antoine, Risk stratification after paracetamol overdose using mechanistic biomarkers: results from two prospective cohort studies, Lancet Gastroenterol. Hepatol. 3 (2) (2018) 104–113, https://doi.org/10.1016/S2468-1253(17)30266-2.

[11] A.G. Madboly, N.F. Alhusseini, S.M. Abd El Rahman, W.B. El Gazzar, A.M.M. Idris, Serum miR-122 and miR-192 as biomarkers of intrinsic and idiosyncratic acute hepatotoxicity: a quantitative real-time polymerase chain reaction study in adult albino rats, J. Biochem. Mol. Toxicol. 33 (7) (2019) e22321, https://doi.org/10.1002/jbt.22321.

[12] F. Precazzini, S. Detassis, A.S. Imperatori, M.A. Denti, P. Campomenosi, Measurements methods for the development of MicroRNA-based tests for cancer diagnosis, Int. J. Mol. Sci. 22 (3) (2021) 1176, https://doi.org/10.3390/ijms22031176.

[13] K.W. Witwer, Circulating MicroRNA biomarker studies: pitfalls and potential solutions, Clin. Chem. 61 (1) (2015) 56–63, https://doi.org/10.1373/clinchem.2014.221341.

[14] K. Saliminejad, H.R.K. Khorshid, S.H. Ghaffari, Why have microRNA biomarkers not been translated from bench to clinic? Future Oncol. 15 (8) (2019) 801–803, https://doi.org/10.2217/fon-2018-0812.

[15] V. Del Vescovo, T. Meier, A. Inga, M.A. Denti, J. Borlak, A cross-platform comparison of affymetrix and Agilent microarrays reveals discordant miRNA expression in lung tumors of c-Raf transgenic mice, PloS One 8 (11) (2013) e78870, https://doi.org/10.1371/journal.pone.0078870.

[16] T. Jet, G. Gines, Y. Rondelez, V. Taly, Advances in multiplexed techniques for the detection and quantification of microRNAs, Chem. Soc. Rev. 50 (6) (2021) 4141–4161, https://doi.org/10.1039/D0CS00609B.

[17] T. Ouyang, Z. Liu, Z. Han, Q. Ge, MicroRNA Detection Specificity: Recent Advances and Future Perspective, Anal. Chem. 91 (5) (2019) 3179–3186, https://doi.org/10.1021/acs.analchem.8b05909.

[18] M. Castelluzzo, A. Perinelli, S. Detassis, M.A. Denti, L. Ricci, MiRNA-QC-and-Diagnosis: An R package for diagnosis based on MiRNA expression, SoftwareX 12 (2020) 100569, https://doi.org/10.1016/j.softx.2020.100569.

[19] Z. Shabaninejad, F. Yousefi, A. Movahedpour, Y. Ghasemi, S. Dokanehiifard, S. Rezaei, R. Aryan, A. Savardashtaki, H. Mirzaei, Electrochemical-based biosensors for microRNA detection: Nanotechnology comes into view, Anal. Biochem. 581 (2019) 113349, https://doi.org/10.1016/j.ab.2019.113349.

[20] F.R. Bowler, J.J. Diaz-Mochon, M.D. Swift, M. Bradley, DNA analysis by dynamic chemistry, Angew. Chem. Int. Ed. 49 (10) (2010) 1809–1812, https://doi.org/10.1002/anie.200905699.

[21] A. Delgado-Gonzalez, A. Robles-Remacho, A. Marin-Romero, S. Detassis, B. Lopez-Longarela, F.J. Lopez-Delgado, D. de Miguel-Perez, J.J. Guardia-Monteagudo, M. A. Fara, M. Tabraue-Chavez, S. Pernagallo, R.M. Sanchez-Martin, J.J. Diaz-Mochon, PCR-free and chemistry-based technology for miR-21 rapid detection directly from tumour cells, Talanta 200 (2019) 51–56, https://doi.org/10.1016/j.talanta.2019.03.039.

[22] A. Marín-Romero, A. Robles-Remacho, M. Tabraue-Chávez, B. López-Longarela, R. M. Sánchez-Martín, J.J. Guardia-Monteagudo, M.A. Fara, F.J. López-Delgado, S. Pernagallo, J.J. Díaz-Mochón, A PCR-free technology to detect and quantify microRNAs directly from human plasma, Analyst 143 (23) (2018) 5676–5682, https://doi.org/10.1039/C8AN01397G.

[23] S. Pernagallo, G. Ventimiglia, C. Cavalluzzo, E. Alessi, H. Ilyine, M. Bradley, J. J. Diaz-Mochon, Novel Biochip Platform for Nucleic Acid Analysis, Sensors 12 (6) (2012) 8100–8111, https://doi.org/10.3390/s120608100.

[24] D.M. Rissin, B. López-Longarela, S. Pernagallo, H. Ilyine, A.D.B. Vliegenthart, J. W. Dear, J.J. Díaz-Mochón, D.C. Duffy, Polymerase-free measurement of microRNA-122 with single base specificity using single molecule arrays: Detection

of drug-induced liver injury, PloS One 12 (7) (2017) e0179669, https://doi.org/10.1371/journal.pone.0179669.
[25] S. Venkateswaran, M.A. Luque-González, M. Tabraue-Chávez, M.A. Fara, B. López-Longarela, V. Cano-Cortes, F.J. López-Delgado, R.M. Sánchez-Martín, H. Ilyine, M. Bradley, S. Pernagallo, J.J. Díaz-Mochón, Novel bead-based platform for direct detection of unlabelled nucleic acids through Single Nucleobase Labelling, Talanta 161 (2016) 489–496, https://doi.org/10.1016/j.talanta.2016.08.072.
[26] B. López-Longarela, E.E. Morrison, J.D. Tranter, L. Chahman-Vos, J.-F. Léonard, J.-C. Gautier, S. Laurent, A. Lartigau, E. Boitier, L. Sautier, P. Carmona-Saez, J. Martorell-Marugan, R.J. Mellanby, S. Pernagallo, H. Ilyine, D.M. Rissin, D. C. Duffy, J.W. Dear, J.J. Díaz-Mochón, Direct Detection of miR-122 in Hepatotoxicity Using Dynamic Chemical Labeling Overcomes Stability and isomiR Challenges, Anal. Chem. 92 (4) (2020) 3388–3395, https://doi.org/10.1021/acs.analchem.9b05449.
[27] A. Marín-Romero, M. Tabraue-Chávez, J.W. Dear, R.M. Sánchez-Martín, H. Ilyine, J.J. Guardia-Monteagudo, M.A. Fara, F.J. López-Delgado, J.J. Díaz-Mochón, S. Pernagallo, Amplification-free profiling of microRNA-122 biomarker in DILI patient serums, using the luminex MAGPIX system, Talanta 219 (2020) 121265, https://doi.org/10.1016/j.talanta.2020.121265.
[28] M. Tabraue-Chávez, M.A. Luque-González, A. Marín-Romero, R.M. Sánchez-Martín, P. Escobedo-Araque, S. Pernagallo, J.J. Díaz-Mochón, A colorimetric strategy based on dynamic chemistry for direct detection of Trypanosomatid species, Sci. Rep. 9 (1) (2019) 3696, https://doi.org/10.1038/s41598-019-39946-0.
[29] A. Robles-Remacho, M.A. Luque-Gonzalez, F.J. López-Delgado, J.J. Guardia-Monteagudo, M.A. Fara, S. Pernagallo, R.M. Sanchez-Martin, J.J. Diaz-Mochon, Direct detection of alpha satellite DNA with single-base resolution by using abasic Peptide Nucleic Acids and Fluorescent in situ Hybridization, Biosens. Bioelectron. 219 (2023) 114770, https://doi.org/10.1016/j.bios.2022.114770.
[30] A. Marín-Romero, M. Tabraue-Chávez, B. López-Longarela, M.A. Fara, R. M. Sánchez-Martín, J.W. Dear, H. Ilyine, J.J. Díaz-Mochón, S. Pernagallo, Simultaneous Detection of Drug-Induced Liver Injury Protein and microRNA Biomarkers Using Dynamic Chemical Labelling on a Luminex MAGPIX System, Analytica 2 (4) (2021) 130–139, https://doi.org/10.3390/analytica2040013.
[31] T.D. Canady, N. Li, L.D. Smith, Y. Lu, M. Kohli, A.M. Smith, B.T. Cunningham, Digital-resolution detection of microRNA with single-base selectivity by photonic resonator absorption microscopy, Proc. Natl. Acad. Sci. U. S. A. 116 (39) (2019) 19362–19367, https://doi.org/10.1073/pnas.1904770116.
[32] E. Garcia-Fernandez, M.C. Gonzalez-Garcia, S. Pernagallo, M.J. Ruedas-Rama, M. A. Fara, F.J. López-Delgado, J.W. Dear, H. Ilyine, C. Ress, J.J. Díaz-Mochón, A. Orte, miR-122 direct detection in human serum by time-gated fluorescence imaging, Chem. Commun. 55 (99) (2019) 14958–14961, https://doi.org/10.1039/C9CC08069D.
[33] E. Garcia-Fernandez, S. Pernagallo, J.A. González-Vera, M.J. Ruedas-Rama, J. J. Díaz-Mochón, A. Orte, Time-Gated Luminescence Acquisition for Biochemical Sensing: miRNA Detection, in: B. Pedras (Ed.), Fluorescence in Industry, Springer International Publishing, Cham, 2019, pp. 213–267, https://doi.org/10.1007/4243_2018_4.
[34] D. Geißler, S. Stufler, H.-G. Löhmannsröben, N. Hildebrandt, Six-Color Time-Resolved Förster Resonance Energy Transfer for Ultrasensitive Multiplexed Biosensing, J. Am. Chem. Soc. 135 (3) (2013) 1102–1109, https://doi.org/10.1021/ja310317n.
[35] X. Qiu, J. Guo, Z. Jin, A. Petreto, I.L. Medintz, N. Hildebrandt, Multiplexed Nucleic Acid Hybridization Assays Using Single-FRET-Pair Distance-Tuning, Small 13 (25) (2017) 1700332, https://doi.org/10.1002/smll.201700332.
[36] X. Qiu, J. Guo, J. Xu, N. Hildebrandt, Three-Dimensional FRET Multiplexing for DNA Quantification with Attomolar Detection Limits, J. Phys. Chem. Lett. 9 (15) (2018) 4379–4384, https://doi.org/10.1021/acs.jpclett.8b01944.
[37] X. Qiu, N. Hildebrandt, Rapid and Multiplexed MicroRNA Diagnostic Assay Using Quantum Dot-Based Förster Resonance Energy Transfer, ACS Nano 9 (8) (2015) 8449–8457, https://doi.org/10.1021/acsnano.5b03364.
[38] J.-C.G. Bünzli, S.V. Eliseeva, Intriguing aspects of lanthanide luminescence, Chem. Sci. 4 (5) (2013) 1939–1949, https://doi.org/10.1039/c3sc22126a.
[39] A. Ruiz-Arias, F. Fueyo-González, C. Izquierdo-García, A. Navarro, M. Gutiérrez-Rodríguez, R. Herranz, C. Burgio, A. Reinoso, J.M. Cuerva, A. Orte, J.A. González-Vera, Exchangeable Self-Assembled Lanthanide Antennas for PLIM Microscopy, Angew. Chem. Int. Ed. 63 (2024) e202314595, https://doi.org/10.1002/anie.202314595.
[40] L. Jiang, D. Duan, Y. Shen, J. Li, Direct microRNA detection with universal tagged probe and time-resolved fluorescence technology, Biosens. Bioelectron. 34 (1) (2012) 291–295, https://doi.org/10.1016/j.bios.2012.01.035.
[41] L. Lu, D. Tu, Y. Liu, S. Zhou, W. Zheng, X. Chen, Ultrasensitive detection of cancer biomarker microRNA by amplification of fluorescence of lanthanide nanoprobes, Nano Res 11 (1) (2018) 264–273, https://doi.org/10.1007/s12274-017-1629-9.
[42] L. Mao, Z. Lu, N. He, L. Zhang, Y. Deng, D. Duan, A new method for improving the accuracy of miRNA detection with NaYF4:Yb,Er upconversion nanoparticles, Sci. China Chem. 60 (1) (2017) 157–162, https://doi.org/10.1007/s11426-016-0021-0.
[43] A. Ruiz-Arias, F. Fueyo-González, C. Izquierdo-García, A. Navarro, M. Gutiérrez-Rodríguez, R. Herranz, C. Burgio, A. Reinoso, J.M. Cuerva, A. Orte, J.A. González-Vera, Exchangeable Self-Assembled Lanthanide Antennas for PLIM Microscopy, Angew. Chem. Int. Ed. (2023) e202314595, https://doi.org/10.1002/anie.202314595 doi: 10.1002/anie.202314595.
[44] T. Nishioka, J. Yuan, Y. Yamamoto, K. Sumitomo, Z. Wang, K. Hashino, C. Hosoya, K. Ikawa, G. Wang, K. Matsumoto, New luminescent europium(III) chelates for DNA labeling, Inorg. Chem. 45 (10) (2006) 4088–4096, https://doi.org/10.1021/ic051276g.
[45] M. Bradley, J.J. Diaz-Mochon, Nucleobase Characterisation, Nucleobase Characterisation (2009) Patent WO 2009/037473 A2. doi:
[46] J. Schindelin, I. Arganda-Carreras, E. Frise, V. Kaynig, M. Longair, T. Pietzsch, S. Preibisch, C. Rueden, S. Saalfeld, B. Schmid, J.-Y. Tinevez, D.J. White, V. Hartenstein, K. Eliceiri, P. Tomancak, A. Cardona, Fiji: an open-source platform for biological-image analysis, Nat. Meth. 9 (7) (2012) 676–682, https://doi.org/10.1038/nmeth.2019.
[47] A. Marín-Romero, M. Tabraue-Chávez, J.W. Dear, J.J. Díaz-Mochón, S. Pernagallo, Open a new window in the world of circulating microRNAs by merging ChemiRNA Tech with a Luminex platform, Sens. Diagn. 1 (6) (2022) 1243–1251, https://doi.org/10.1039/D2SD00111J.
[48] J. Jia, P. Ren, H. Hu, N. Sayyadi, F. Parvin, X. Zheng, B. Shi, J.A. Piper, B. Song, K. Vickery, Y. Lu, Lifetime Multiplexing with Lanthanide Complexes for Luminescence In Situ Hybridisation, Anal. Sens. 2 (2) (2022) e202100057, https://doi.org/10.1002/anse.202100057.
[49] T.Y. Goh, S.N. Basah, H. Yazid, M.J. Aziz Safar, F.S. Ahmad Saad, Performance analysis of image thresholding: Otsu technique, Measurement 114 (2018) 298–307, https://doi.org/10.1016/j.measurement.2017.09.052.
[50] H. Ahmadi, T.L. Jang, S. Daneshmand, S. Ghodoussipour, MicroRNA-371a-3p as a blood-based biomarker in testis cancer, Asian J. Urol. 8 (4) (2021) 400–406, https://doi.org/10.1016/j.ajur.2021.08.004.
[51] K.-P. Dieckmann, A. Radtke, L. Geczi, C. Matthies, P. Anheuser, U. Eckardt, J. Sommer, F. Zengerling, E. Trenti, R. Pichler, H. Belz, S. Zastrow, A. Winter, S. Melchior, J. Hammel, J. Kranz, M. Bolten, S. Krege, B. Haben, W. Loidl, C.G. Ruf, J. Heinzelbecker, A. Heidenreich, J.F. Cremers, C. Oing, T. Hermanns, C. D. Fankhauser, S. Gillessen, H. Reichegger, R. Cathomas, M. Pichler, M. Hentrich, K. Eredics, A. Lorch, C. Wülfing, S. Peine, W. Wosniok, C. Bokemeyer, G. Belge, Serum Levels of MicroRNA-371a-3p (M371 Test) as a New Biomarker of Testicular Germ Cell Tumors: Results of a Prospective Multicentric Study, J. Clin. Oncol. 37 (16) (2019) 1412–1423, https://doi.org/10.1200/jco.18.01480.
[52] K.P. Dieckmann, M. Spiekermann, T. Balks, I. Flor, T. Löning, J. Bullerdiek, G. Belge, MicroRNAs miR-371-3 in serum as diagnostic tools in the management of testicular germ cell tumours, Br. J. Cancer 107 (10) (2012) 1754–1760, https://doi.org/10.1038/bjc.2012.469.
[53] S. Svasti, S. Masaki, T. Penglong, Y. Abe, P. Winichagoon, S. Fucharoen, T. Umemura, Expression of microRNA-451 in normal and thalassemic erythropoiesis, Ann. Hematol. 89 (10) (2010) 953–958, https://doi.org/10.1007/s00277-010-0980-7.
[54] M. Khordadmehr, F. Jigari-Asl, H. Ezzati, R. Shahbazi, S. Sadreddini, S. Safaei, B. Baradaran, A comprehensive review on miR-451: A promising cancer biomarker with therapeutic potential, J. Cell. Physiol. 234 (12) (2019) 21716–21731, https://doi.org/10.1002/jcp.28888.
[55] X.-F. Zhang, J. Zhang, L. Liu, Fluorescence Properties of Twenty Fluorescein Derivatives: Lifetime, Quantum Yield, Absorption and Emission Spectra, J. Fluoresc. 24 (3) (2014) 819–826, https://doi.org/10.1007/s10895-014-1356-5.
[56] M.K. Singh, Time-resolved single molecule fluorescence spectroscopy of Cy5-dCTP: influence of the immobilization strategy, Phys. Chem. Chem. Phys. 11 (33) (2009) 7225–7230, https://doi.org/10.1039/b821632k.
[57] F. Bian, J. Wu, H. Wang, L. Sun, C. Shao, Y. Wang, Z. Li, X. Wang, Y. Zhao, Bioinspired Photonic Barcodes with Graphene Oxide Encapsulation for Multiplexed MicroRNA Quantification, Small 14 (52) (2018) 1803551, https://doi.org/10.1002/smll.201803551.
[58] L. Chen, G. Hu, B. Cui, J. Gao, X. Gu, H. Cui, Z. Zeng, Development of a stable and efficient fluorescence nanosensor for in situ detection of MicroRNA in plant, Sens. Actuat. B-Chem. 404 (2024) 135244, https://doi.org/10.1016/j.snb.2023.135244.
[59] A. Roychoudhury, J.W. Dear, M. Kersaudy-Kerhoas, T.T. Bachmann, Amplification-free electrochemical biosensor detection of circulating microRNA to identify drug-induced liver injury, Biosens. Bioelectron. 231 (2023) 115298, https://doi.org/10.1016/j.bios.2023.115298.
[60] H. Shen, Z. Li, B. Dou, Q. Feng, P. Wang, An amplified logic gate driven by in situ synthesis of silver nanoclusters for identification of biomarkers, Chem. Commun. 59 (38) (2023) 5705–5708, https://doi.org/10.1039/D3CC00643C.
[61] A. Chen, S. Ma, Y. Zhuo, Y. Chai, R. Yuan, In Situ Electrochemical Generation of Electrochemiluminescent Silver Naonoclusters on Target-Cycling Synchronized Rolling Circle Amplification Platform for MicroRNA Detection, Anal. Chem. 88 (6) (2016) 3203–3210, https://doi.org/10.1021/acs.analchem.5b04578.
[62] K. Zhang, H. Zhang, H. Cao, Y. Jiang, K. Mao, Z. Yang, Rolling Circle Amplification as an Efficient Analytical Tool for Rapid Detection of Contaminants in Aqueous Environments, Biosensors 11 (10) (2021) 352, https://doi.org/10.3390/bios11100352.
[63] H. Wang, M. Shen, X. Shen, J. Liu, W. Huang, X. Jiang, H. Liu, S. Zeng, K. Nan, S. Cai, An enzyme-free sensing platform for miRNA detection and in situ imaging in clinical samples based on DNAzyme cleavage-triggered catalytic hairpin assembly, Biosens. Bioelectron. 256 (2024) 116279, https://doi.org/10.1016/j.bios.2024.116279.
[64] C. Fan, L. Xie, F. Zhao, J. Wang, X. Lin, X. Chen, Novel fluorescence nano-orbital biosensor for highly sensitive microRNA detection, Anal. Chim. Acta 1288 (2024) 342172, https://doi.org/10.1016/j.aca.2023.342172.
[65] F. Qi, Y. Ju, Y. Xiong, J. Lu, Y. Zhang, Ultrasensitive fluorescence microRNA biosensor by coupling hybridization-initiated exonuclease I protection and tyramine signal amplification, Talanta 272 (2024) 125777, https://doi.org/10.1016/j.talanta.2024.125777.
[66] H. Yang, D. Chen, Y. Zhang, P. Yuan, N. Xie, Z. Dai, MiRNA and mRNA-Controlled Double-Cascaded Amplifying Circuit Nanosensor for Accurate Discrimination of

Breast Cancers in Living Cells, Animals, and Organoids, Anal. Chem. 96 (10) (2024) 4154–4162, https://doi.org/10.1021/acs.analchem.3c05085.
[67] D. Li, Y. Liu, Y. Li, Y. Xiang, R. Yuan, Simultaneous and Sensitive Sensing of Intracellular MicroRNA and mRNA for the Detection of the PI3K/AKT Signaling Pathway in Live Cells, Anal. Chem. 96 (8) (2024) 3329–3334, https://doi.org/10.1021/acs.analchem.3c04135.
[68] C. Liu, X. Wei, H. Zhang, M. Zhang, X.-F. Yu, N. Hildebrandt, Q.-Y. Luo, Z. Jin, Nucleic Acid Hybridization Enhanced Luminescence for Rapid and Sensitive RNA and DNA Based Diagnostics, Anal. Chem. 94 (46) (2022) 15964–15970, https://doi.org/10.1021/acs.analchem.2c02673.
[69] S. Joo, U.J. Lee, H.Y. Son, M. Kim, Y.-M. Huh, T.G. Lee, M. Lee, Highly Selective FRET-Aided Single-Molecule Counting of MicroRNAs Labeled by Splinted Ligation, ACS Sens. 7 (11) (2022) 3409–3415, https://doi.org/10.1021/acssensors.2c01526.
[70] R. Datta, T.M. Heaster, J.T. Sharick, A.A. Gillette, M.C. Skala, Fluorescence lifetime imaging microscopy: fundamentals and advances in instrumentation, analysis, and applications, J. Biomed. Opt. 25 (7) (2020) 071203, https://doi.org/10.1117/1.JBO.25.7.071203.
[71] C. Guzmán, C. Oetken-Lindholm, D. Abankwa, Automated High-Throughput Fluorescence Lifetime Imaging Microscopy to Detect Protein–Protein Interactions, SLAS Technol. 21 (2) (2016) 238–245, https://doi.org/10.1177/2211068215606048.
[72] M. Padial-Jaudenes, M. Tabraue-Chávez, S. Detassis, M.J. Ruedas-Rama, Md.C. González-García, M.A. Fara, F.J. López-Delgado, J.A. González-Vera, J.J. Guardia-Monteagudo, J.J. Díaz-Mochón, E. García-Fernández, S. Pernagallo, A. Orte, Dataset from article 'Multiplexed micro-RNA Biomarker Detection by Bridging Lifetime Filtering Imaging and Dynamic Chemistry Labeling'. DOI:10.30827/Digibug.84916, 2023.

Maria Padial-Jaudenes. Degree in Food Science at the University of Granada (Spain) and, formerly, researcher at the Department of Physical Chemistry of the Faculty of Pharmacy at the University of Granada (Spain).

Mavys Tabraue-Chávez works as the Chief Scientific Officer at DESTINA Genomica SL in Spain. She earned her PhD in Pharmacy from the University of Granada, where her research focused on designing and synthesizing new HDAC inhibitors for use as anticancer drugs. Her expertise encompasses chemical synthesis, microencapsulation, biosensors, biomaterials, as well as scaling up and optimizing processes.

Simone Detassis works as assay development manager at OPTOI SRL (Italy). He earned his PhD Europeaus in Biomolecular Sciencies from the University of Trento with a focus on innovative analytical methods for nucleic acids detections and miRNAs as biomarkers for lung and prostate cancer. His expertise spans from molecular biology to analytical chemistry.

Maria J. Ruedas-Rama is full Professor in Physical Chemistry at the Faculty of Pharmacy of the University of Granada (Spain). Her main research lines lie in the use of luminescent nanoparticles and other nanotechnological platforms for developing biomedical sensing strategies.

M. Carmen Gonzalez-Garcia is currently a postdoctoral researcher at IMDEA Nanoscience (Madrid, Spain). Her research interests are focused on the design, development, and application of new luminescent sensors for intracellular processes and biomarker detection.

Mario Antonio Fara works as a Senior Chemistry Scientist at DESTINA Genomica SL, Spain. In this role, he is responsible for designing, synthesizing, purifying, and characterizing DESTINA's reagents specifically for PCR-Free interrogation of circulating nucleic acids in liquid biopsies. His primary research interests include solid-phase synthesis, nucleic acid analysis, dynamic chemistry, and organic synthesis.

F. Javier López-Delgado is currently a Chemistry Scientist at DESTINA Genomica SL (Spain), where he designs, synthesizes, purifies, and characterizes SMART-Bases. His main research interests encompass solid-phase synthesis, nucleic acid analysis, dynamic chemistry, organic synthesis, and natural product chemistry.

Juan A. González-Vera is currently Associate Professor in the Physical Chemistry Department at the Faculty of Pharmacy of the University of Granada (Spain). His main research interests are directed to the development of luminescent tools for the study of complex biological systems at the interface of chemistry and biology.

Juan J. Guardia-Monteagudo is currently a Chemistry Scientist at DESTINA Genomica SL (Spain), where he designs, synthesizes, purifies, and characterizes DGL probes. His main research interests encompass solid-phase synthesis, nucleic acid analysis, dynamic chemistry, organic synthesis, and natural product chemistry.

Juan J. Diaz-Mochon is an Associate Professor in the Department of Pharmaceutical and Organic Chemistry at the Faculty of Pharmacy, located at the University of Granada, Spain. His research focus on the development of cutting-edge therapeutic and diagnostic tools, utilizing the principles of nanotechnology, biomaterials, peptide nucleic acids and dynamic chemistry. A basis of his approach is the deep collaboration with clinicians, aiming to significantly enhance the wellbeing and quality of life for people.

Emilio Garcia-Fernandez: is currently Associate Professor in the Physical Chemistry Department at the Faculty of Pharmacy of the University of Granada (Spain). His research interests include the development of fluorescence sensors for biomedical, nanotechnological and food applications; fluorescence imaging microscopy, photochemistry, photophysics and related fields.

Salvatore Pernagallo currently serves as the Chief Technology Officer at DESTINA Genomica SL in Spain and is the coordinator of the European project, diaRNAgnosis (GA - ID: 101007934), which provides funding for this research. His main research focus is on identifying new biomarkers, including both proteins and nucleic acids, in liquid biopsies and creating innovative tools for their analysis. Furthermore, he has extensive expertise in nano-systems for drug delivery, coupled with a deep understanding of biochemistry, molecular biology, and sequencing technologies.

Angel Orte is currently full Professor in Physical Chemistry at the Faculty of Pharmacy of the University of Granada (Spain), and head of the Nanoscopy-UGR Singular Lab and the 'FQM247-Photochemistry and Photobiology' research group. His main research interests are devoted to development of advanced fluorescence microscopy and single-molecule fluorescence tools for the study of biomedical problems, such as protein aggregation and pathological cellular processes.